

1  
2  
3  
4  
5  
6  
7  
8  
9  
10  
11  
12  
13  
14  
15  
16  
17

Supplementary Material for  
**Local Atmospheric Decoupling in Complex Topography Alters Climate  
Change Impacts**

Christopher Daly,\* David R. Conklin, and Michael H. Unsworth

\*To whom correspondence should be addressed. E-mail: [daly@nacse.org](mailto:daly@nacse.org)

This supplement contains:

- Atmospheric Circulation Analysis
- Topographic Index
- References
- Figures
  - S1. 700-hPa upper-air grid points of the NCEP/NCAR reanalysis
  - S2. Spatial patterns of topographic index in the HJA

18

19

## Supplementary Online Material

20

### 21 **Atmospheric Circulation Analysis**

22 An atmospheric flow strength and curvature analysis was conducted for the H.J. Andrews

23 Experimental Forest. In an initial analysis, flow characteristics at the 700-hPa (~3000-m) level

24 were found to have strong explanatory power for surface temperature, and were used here.

25 Pressure height data from the NCEP/NCAR Reanalysis (Kalnay et al. 1996) were used to

26 quantify the geostrophic flow strength and curvature at 4 AM and 4 PM PST daily for the period

27 1987-2005. Flow characteristics at 4 AM (12 UTC) represented the daily minimum temperature,

28 and those at 4 PM PST (00 UTC+1 day) represented the daily maximum temperature.

29 The circulation analysis included deriving three flow strength indices: southerly flow

30 component ( $S$ ), westerly flow component ( $W$ ), and overall strength of the flow ( $F$ ; Losleben et al.

31 2000). Days on which  $F$  fell into the lower one-third of the distribution of all daily flow

32 strengths for this location were designated low flow days, medium for the middle third, and high

33 for the upper third. Also calculated were three flow vorticity (or curvature) indices: southerly

34 vorticity component ( $ZS$ ), westerly vorticity component ( $ZW$ ), and total vorticity of the flow ( $Z$ ).

35 Each day was assigned to a zonal, cyclonic, or anticyclonic flow curvature category based on the

36 sign of  $Z$  and a comparison of the magnitudes of  $Z$  and  $F$ .

37 The analysis used grid points spaced 5 degrees apart over the western U.S. and northeast

38 Pacific, centered on 45°N and 122.5°W. Fig. S2 shows numbered grid points whose 700-hPa

39 pressure heights were used to calculate circulation indices. Points are labeled  $p_1$  through  $p_{25}$  as

40 shown. In the following formulas, the variables  $cc$ ,  $sc$ ,  $c_1$ , and  $c_2$  account for differing grid  
 41 spacing in the latitudinal and longitudinal directions.

42 Southerly flow component ( $S$ ) =  $cc \left( \frac{p_9 + 2p_{14} + p_{19}}{4} - \frac{p_7 + 2p_{12} + p_{17}}{4} \right)$

43 where  $cc = \frac{1}{\cos(lat)}$

44 Westerly flow component ( $W$ ) =  $\frac{p_{17} + 2p_{18} + p_{19}}{4} - \frac{p_7 + 2p_8 + p_9}{4}$

45 Mean flow strength ( $F$ ) =  $\sqrt{S^2 + W^2}$

46 Southerly vorticity component ( $ZS$ ) =

47  $sc \left( \frac{p_{10} + 2p_{15} + p_{20}}{4} - \frac{p_8 + 2p_{13} + p_{18}}{4} - \frac{p_8 + 2p_{13} + p_{18}}{4} + \frac{p_6 + 2p_{11} + p_{16}}{4} \right)$

48 where  $sc = \frac{1}{2(\cos(lat))^2}$

49

50 Westerly vorticity component ( $ZW$ ) =

51  $c_1 \left( \frac{p_{22} + 2p_{23} + p_{24}}{4} - \frac{p_{12} + 2p_{13} + p_{14}}{4} \right) - c_2 \left( \frac{p_{12} + 2p_{13} + p_{14}}{4} - \frac{p_2 + 2p_3 + p_4}{4} \right)$

52 where  $c_1 = \frac{\sin(lat)}{\sin(lat - 5)}$ ,  $c_2 = \frac{\sin(lat)}{\sin(lat + 5)}$ , and  $lat = 45$  degrees latitude

53

54 Total vorticity ( $Z$ ) =  $ZS + ZW$

55

56 Flow curvature = 
$$\left\{ \begin{array}{l} \text{Zonal}; |Z| < F \\ \text{Cyclonic}; |Z| > F, Z > 0 \\ \text{Anticyclonic}; |Z| > F, Z < 0 \end{array} \right\}$$

57

58 **Topographic Index**

59 A “topographic index” grid was created for the HJA, which describes the height of a  
 60 pixel relative to nearby terrain features. Topographic index provides information on a site’s  
 61 susceptibility to cold air pooling by considering its vertical position relative to the surrounding  
 62 terrain (Daly et al. 2007, 2008). Stations located in deep valleys and depressions are more  
 63 susceptible to cold air pooling than those located on slopes or ridge tops.

64 The process of creating a topographic index grid is a two-dimensional analog to using a  
 65 high-pass filter to remove low frequency variations from a signal. The topographic index grid is  
 66 a new map from which the larger (more “slowly” varying in space) features have been removed,  
 67 leaving only an elevation relative to other nearby points.

68 For each pixel in a 50-m DEM, the pixel with the lowest elevation within a given search  
 69 diameter was found, and a grid created from these lowest pixels. Each pixel in this minimum-  
 70 elevation grid was then subjected to an algorithm that averaged all pixels within a diameter equal  
 71 to the search diameter, thus creating a third grid. Finally, this averaged minimum-elevation grid  
 72 was subtracted from the original DEM to produce the topographic index grid.

73 Topographic index grids with search/averaging diameters of 150, 250, 400, and 500 m  
 74 were calculated, and each entered with elevation as explanatory variables in the multiple  
 75 regression function to predict the A-C slope for December  $T_{\max}$ . The search/averaging diameter  
 76 of 150 m had the greatest explanatory power, and was used in the final analysis (Fig. S2). This is

77 the smallest possible diameter that could be used with the 50-m DEM (constituting three 50-m  
78 pixels), leaving open the possibility that the use of finer-resolution DEMs and smaller diameters  
79 could produce topographic index grids with even more explanatory power. The HJA Long-Term  
80 Ecological Research Program has sponsored the creation of a very fine resolution DEM of the  
81 HJA using LIDAR (Light Detection and Ranging) technology; this DEM will allow us to  
82 investigate possible finer-scale topographic interactions. However, it is likely that multiple  
83 scales will need to be considered. Cold air drainage appears to be fractal in nature, exhibiting  
84 patterns within patterns at scales ranging from large valleys that are tens of km wide to narrow  
85 ravines of no more than a few meters in width (Daly et al. 2008).

86

#### 87 **Literature Cited**

88

89 Daly, C, Halbleib, MD, Smith, JI, Gibson, WP, Doggett, MK, Taylor, GH, Curtis, J, Pasteris, P.  
90 2008. Physiographically-sensitive mapping of temperature and precipitation across the  
91 conterminous United States. *International Journal of Climatology*, 28, 2031-2064.

92

93 Daly C, Smith JW, Smith JI, McKane R. 2007. High-resolution spatial modeling of daily  
94 weather elements for a catchment in the Oregon Cascade Mountains, United States.  
95 *Journal of Applied Meteorology and Climatology* 46, 1565-1586.

96

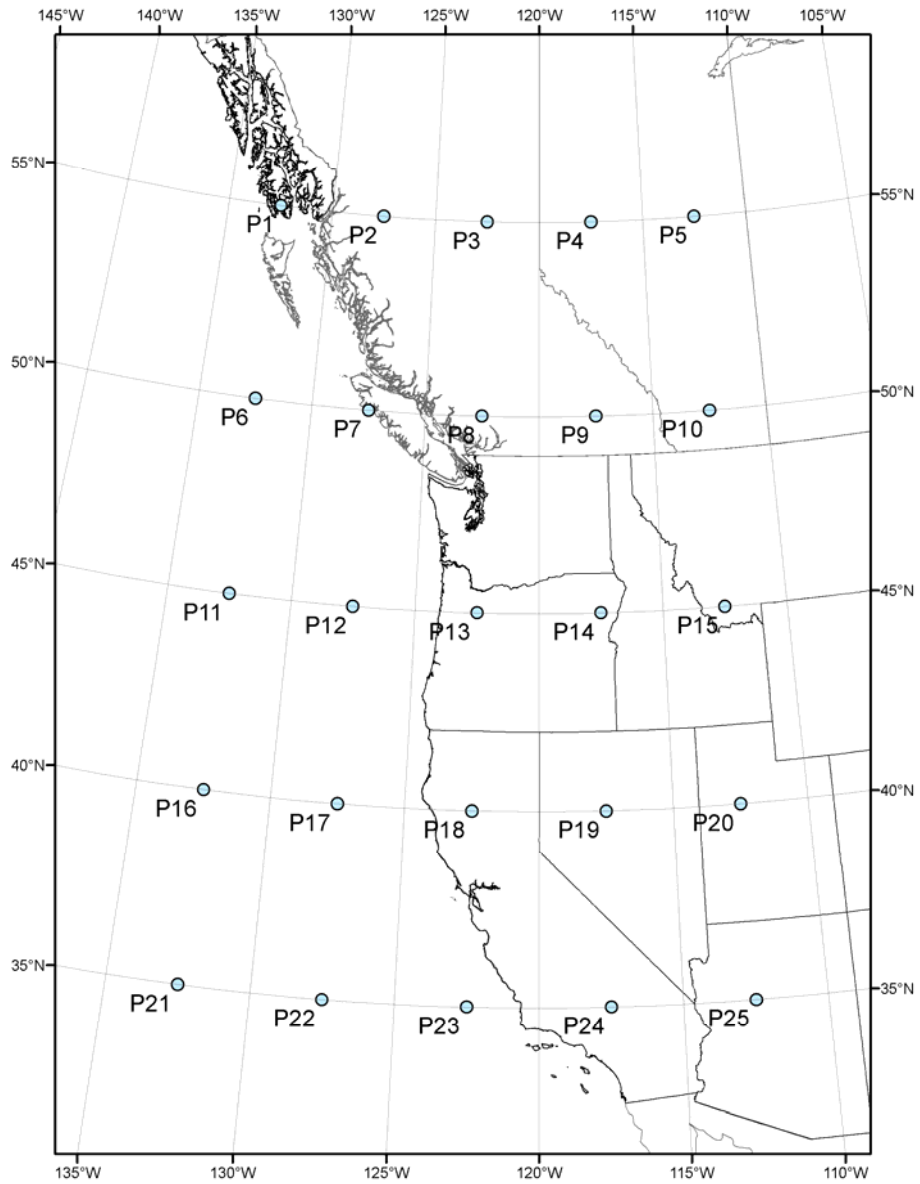
97 Kalnay E, et al. 1996. The NCEP/NCAR 40-year reanalysis project. *Bull. Amer. Meteor. Soc.*  
98 77, 437-470.

99

100 Losleben M, Pepin N, Pedrick S. 2000. Relationships of precipitation chemistry, atmospheric  
101 circulation, and elevation, at two sites on the Colorado Front Range. *Atmospheric*  
102 *Environment* 34, 1723-1737.

103  
104

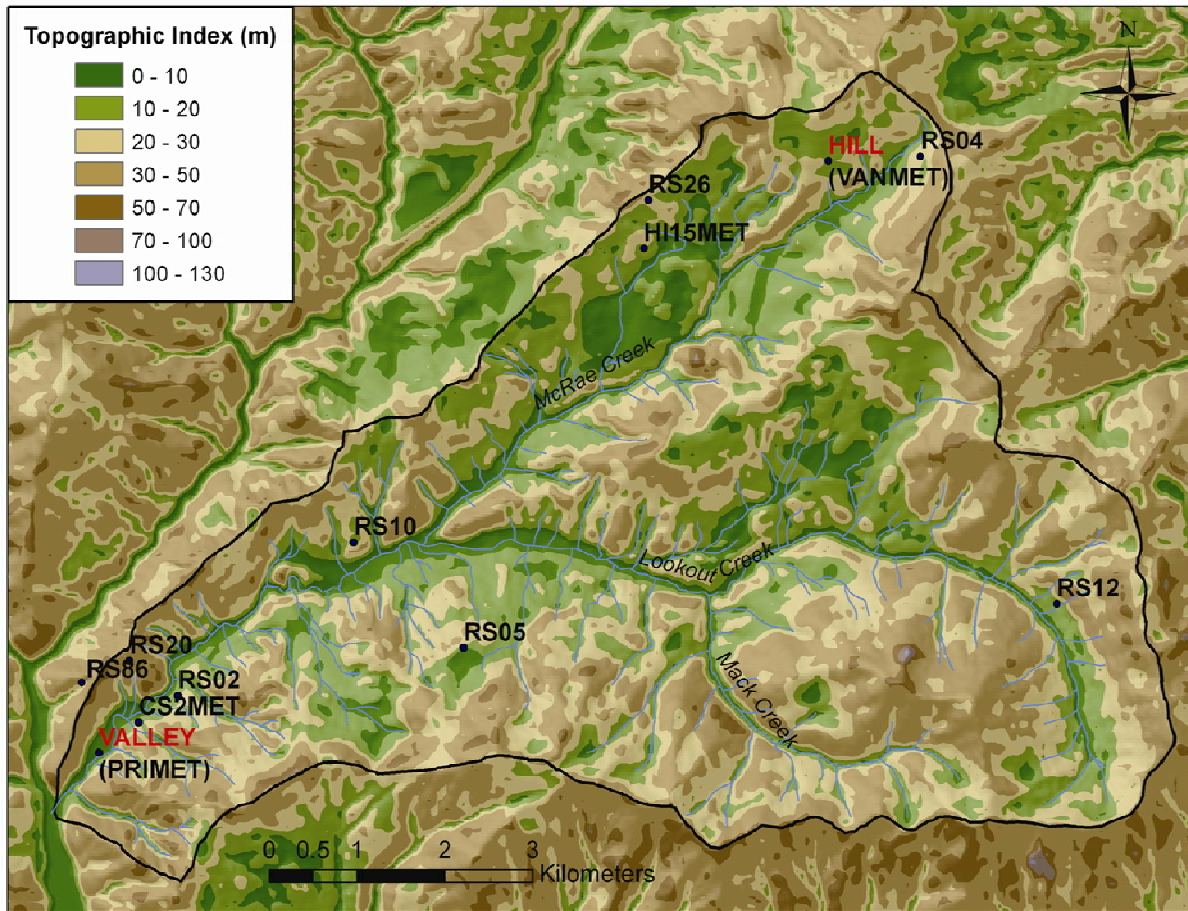
105  
106  
107  
108



109  
110  
111  
112

**Figure S1.** 700-hPa grid points of the NCAR/NCEP reanalysis used in the atmospheric circulation analysis.

113  
114  
115  
116  
117



118  
119  
120  
121  
122  
123  
124  
125  
126  
127  
128

**Figure S2.** Spatial patterns of topographic index in the HJA. Index value at each pixel is the height of that pixel relative to the generalized lowest terrain within 150 m (see text). Locations of stations used in the analysis, including VALLEY (PRIMET) and HILL (VANMET), are shown.